JPhys Energy

Effectiveness of poly(methyl methacrylate) spray encapsulation for perovskite solar cells

Journal of Physics: Energy

PAPER

Effectiveness of poly(methyl methacrylate) spray encapsulation for perovskite solar cells

Declan Hughes[1,*], Michael Spence[1], Suzanne K Thomas[1], Rokas Apanavicius[1], Chris Griffiths[2], Matthew J Carnie[1] and Wing C Tsoi[1,*]

[1] SPECIFIC-IKC, Department of Materials Science and Engineering, Swansea University, Bay Campus, Fabian Way, Swansea SA1 8EN, United Kingdom
[2] SPECIFIC PMRC (Pilot Manufacturing Research Centre), 24–26 Mardon Park, Central Ave, Port Talbot SA12 7AX, United Kingdom
* Authors to whom any correspondence should be addressed.

E-mail: 823426@swansea.ac.uk and W.C.Tsoi@swansea.ac.uk

Keywords: encapsulation, perovskite, stability, lightweight, spray-coating

Supplementary material for this article is available online

OPEN ACCESS

RECEIVED
27 September 2023

REVISED
28 November 2023

ACCEPTED FOR PUBLICATION
22 January 2024

PUBLISHED
1 February 2024

Abstract

For commercial applications, Perovskite Solar Cells (PSCs) need to be well encapsulated to improve long term stability. The most common method, glass-glass encapsulation, uses edge sealant materials to encapsulate the device between sheets of glass. Glass-Glass encapsulation, while providing provide adequate protection from the ambient environment, limits the use of flexible substrates for thin film solar cells due to its rigidity. Additionally, the added weight of glass encapsulation reduces the specific power (W kg^{-1}) of PSCs, which is an important factor when designing solar cells for aerospace applications. Here we demonstrate that commercially available acrylic spray encapsulation offers efficient and robust stability for PSCs. It is shown that applying the encapsulation via this method does not degrade the PSCs, unlike other literature and glass-glass encapsulation methods. Additionaly, it is shown that 1 coat of acrylic spray encapsulation has an effective thickness of ∼1.77 μm and a weight of ∼6 mg. For stability measurements, PSCs with an acrylic coating show a 4% increase in performance after ∼730 h under dark storage conditions and retain 88% of their initial power conversion efficiency after 288 h under 85% relative humidity 25 °C. We anticipate our assay to be a starting point for further studies into spray encapsulation materials and methods not just for terrestial applications, but for aerospace applications as well.

1. Introduction

Life cycle assessments and economic analysis of Perovskite Solar Cells (PSCs) [1, 2], have indicated that reducing or delaying degradation, and therefore extending the lifetime of operational PSCs, is essential for long term sustainability and viability. Since the highest PSC efficiencies are now competitive with more commonly used PV technologies, the limiting factor on the success of PSCs now lies in their stability. To ensure that PSCs are commercially viable and profitable, PSC lifetimes should be at least 15 years [2], but 25 years stability should be ultimately realized [3]. The solution to improved stability, however, is not so straightforward. On Earth, perovskite's degrade readily when exposed to oxygen and moisture [4–7].

This holds true for terrestrial applications, but also aerospace applications as well. This is because aerospace solar cells are often held in storage before payload launches, meaning the PSCs must also be stable during this wait period. Additionally, a lightweight encapsulation is preferred as the lower weight will lead to a high specific power (W kg^{-1}), which is more appealing for applications such as aerospace, where lower payload weight is more cost effective. Therefore, strategies for lightweight degradation mitigation or prevention are necessary.

A commonly used encapsulation technique for PSCs is glass–glass encapsulation [8]. Various work has shown the effectiveness of glass-glass encapsulation for use with PSCs [9–12], especially when coupled with polyimide tape and UV-cured epoxy [13]. However, glass-glass encapsulation results in rigid PSCs, removing

the use of flexible substrates for solar cells and scale up manufacturing techniques such as roll-2-roll. Due to the weight of of the glass substrate and glass encapsulation, it also greatly decreases the specific power of the devices. Thin film encapsulation methods have been shown to also meet the encapsulation requirements [14, 15], along with allowing for the use of flexible substrates. A promising material in this group is Poly(methyl methacrylate) (PMMA).

PMMA, also known as acrylic, is a commonly used transparent thermoplastic with good impact strength and a glass transition temperature of 108 °C [16]. Given these properties, PMMA has seen commercial up take in replacing glass as a lightweight, shatter-resistant glass alternative since the 1930's [17, 18]. While a major focus is for scalable PMMA sheets, such as Perspex®, PMMA is also dissolvable in many organic solvents allowing for the creation of PMMA inks and coatings [19]. Solution processed PMMA encapsulation has largely taken the form of spin-coated encapsulation layers for perovskite and organic solar cells [20, 21]. PMMA has also shown promising potential as an interlayer to passivate defects in perovskite films [22]. A PMMA interlayer was recently added to PSCs via spin coating to improve the device efficiency and stability in leu of a Copper(II) 2, 9, 16, 23-tetra-tert-butyl-29H, 31H-phtalocyanine (CuPc) hole transporting layer [23]. PMMA encapsulation has the potential to provide a cheap, lightweight, and flexible encapsulation alternative to glass–glass; however the reported fabrication methods of the encapsulation is typically spin-coating with harmful solvents [20]. Therefore, assessing the potential for up scaling is challenging. A robust, lightweight, and scalable PMMA encapsulation technique enabling large area encapsulation and long-term stability for PSCs would clearly be helpful.

In this work, we present a study on the encapsulation potential of commercially available PMMA conformal coating spray. Spray coated PMMA is widely used as a 'conformal coating' in the electronics industry for encapsulating sensitive components on Printed Circuit Boards (PCBs). Many manufacturers also provide similar PMMA encapsulants in bulk for use in automated spray coating setups for high volume production [24]. At a price of ∼£0.05 ml^{-1}, this spray encapsulation offers a very cost-effective encapsulation technique, while also maintaining device performance after the encapsulation is applied. We show a calculation of thin film thickness through profilometry and Raman spectroscopy measurements. Additionally, at the maximum sprayed thickness the encapsulation layer has a weight of ∼15 mg, therefore greatly improving the specific power of the solar cells. We demonstrate ∼730 h of ambient (ISOS-D1) condition stability, with 0% loss in device performance, and a T_{88} of ∼288 h at 85% RH 25 °C.

2. Results and discussion

2.1. Post-encapsulation device performance

It has been demonstrated that the application of encapsulation can degrade the performance of PSCs due to interactions between the encapsulate and inter-layers such as the electrodes or HTL [25]. In previous work, degradation after spin coating PMMA is due to the solvents in which the polymer is dissolved in such as Chlorobenzene (CB) or Toluene, which are also used to dissolve Hole Transporting Materials (HTMs) such as spiro-OMeTAD [26]. Here, the PMMA is dissolved in a mixture of solvents including ethyl acetate, *n*-Butyl acetate, and *n*-Butyl methacrylate. Attention was drawn to the inclusion of ethyl acetate as it can also be used to dissolve spiro-OMeTAD [27], however ethyl acetate possess a higher vapour pressure than CB, and therefore should more readily evaporates after spraying. This may limit the potential degradation of the HTM and should maintain the performance of the devices after encapsulation. The vapour pressure is further increased by heating the devices to 55 °C during the spray coating (see methods).

In figure 1, we show the performance of standard planar PSCs before and after the application of 1 coat (2 sprays) of PMMA encapsulation. The tabulated data that leads to figure 1 is shown in the supplementary information (SI) table S.1. After encapsulation, it appears the overall PCE of the devices remains largely unchanged. Here the average PCE after encapsulation is 13%, a ∼2% change from the initial average of 13.28%. Due to issues of shadowing from the spray mask, the pixel count after encapsulation was reduced by 2. This showcases the importance of the mask, as the PMMA encapsulation layer is a good insulator, and can easily prevent electrode contact. The V_{oc} remained exceedingly consistent after the PMMA was applied. The average V_{oc} before encapsulation was 1.030 V. After encapsulation, a decrease to 1.027 V (<1% decrease) is observed. The average FF decreases from 63.07 to 61.63% after encapsulation (2% decrease). There is a small increase in the measured J_{sc} from an average of 20.36 $mAcm^{-2}$ before encapsulation, to 20.63 $mAcm^{-2}$ after encapsualtion is completed (1% increase). Therefore, it is observed that the application of PMMA encapsulation results in a negligible change in the performance of *n-i-p* planar PSCs. For glass encapsulation, presented in figure S.1 and table S.2 in the SI, the application of Kapton tape/UV epoxy/glass degrades the overall performance of the PSCs, resulting in an overall 20% decrease in PCE, driven by a 19% reduction in FF. Therefore, the PMMA encapsulation offers better PCE retention after encapsulation, especially when

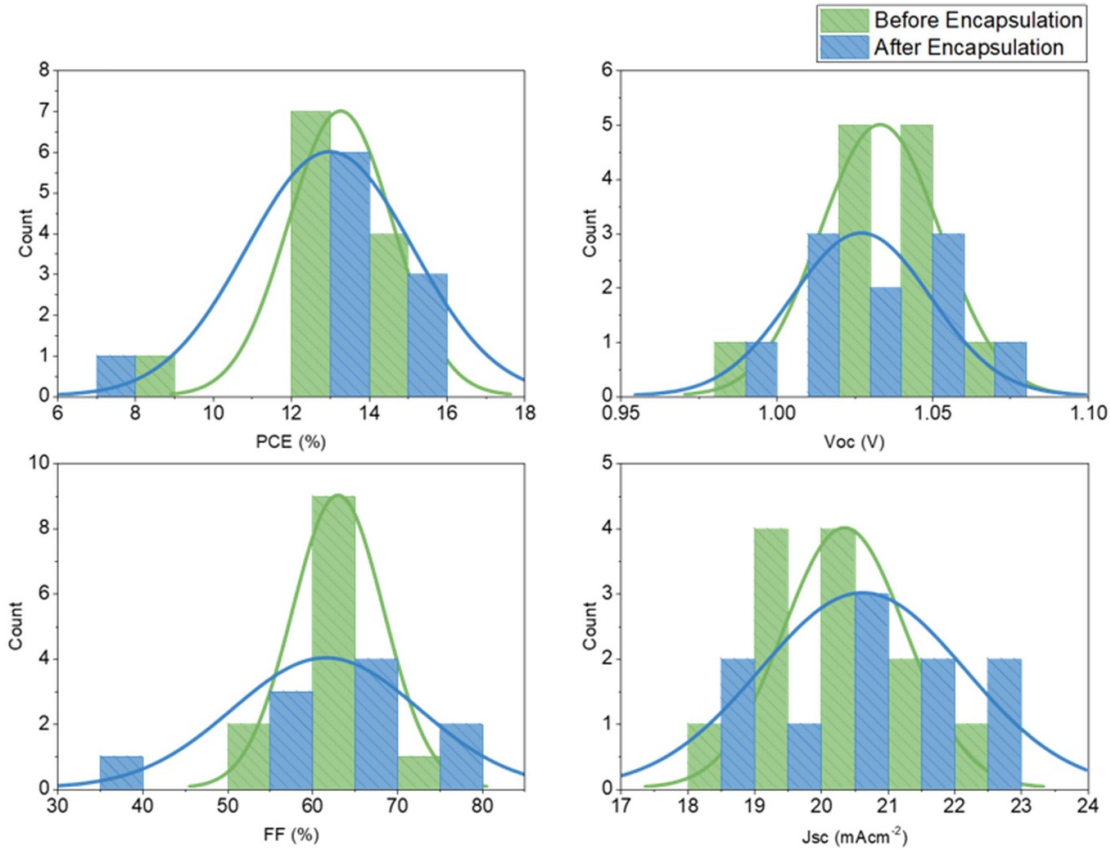

Figure 1. Photovoltaics (PV) parameters for PSCs before and after the application of 1 coat of the PMMA spray encapsulation with normal distribution fitting curves.

compared to previous work with Chlorobenzene [20] and the glass-glass encapsulation presented in figure S.1.

2.2. Encapsulation thickness

Due to the polymer nature of PMMA, water and oxygen can permeate through the material and into layers underneath. The rate of permeation for water and oxygen are the Water Vapour Transfer Rate (WVTR), and the Oxygen Transmission Rate (OTR) respectively. While the presence of oxygen has conflicting effects on the performance of PSCs, such as improving the performance through the passivating of defects [4], and degradation of PSCs through the formation of Pb–O [5]; moisture degradation is a much more prominent issue for PSCs [6]. Both the WVTR and OTR follow an inverse relationship with the material thickness 'L' as shown in equations (1) and (2).

$$\mathrm{WVTR} = \frac{P_0\,(P_2 - P_1)}{L} \mathrm{e}^{\frac{-E_a}{RT}} \tag{1}$$

where P_0 is the permeation coefficient, $(P_2–P_1)$ is the pressure difference between the vapour and the polymer, E_a is the activation energy of the material, R is the ideal gas constant and T is the absolute temperature [28].

$$\mathrm{OTR} = D \cdot S \cdot \frac{P_{\mathrm{atm}} - P_0}{L} \tag{2}$$

where D is the diffusion coefficient, S is the solubility coefficient, and $P_{atm}–P_0$ is the pressure difference across the membrane [28].

Therefore, the thicker the PMMA encapsulation layer, the less ingress of oxygen and moisture through the film at constant temperature. This in practise should present itself as better stability with a thicker encapsulation. As the solar cells can be in storage for long periods of time, characterising the encapsulation thickness is very important as it can affect the storage stability. The PMMA was spray coated onto a variety of different substrates and devices to probe the effect of substrate on thickness and homogeneity. For 1 coat PMMA, there is a large variation in the thickness when coated on the PSCs (figure S4). Figure 2(a) shows the

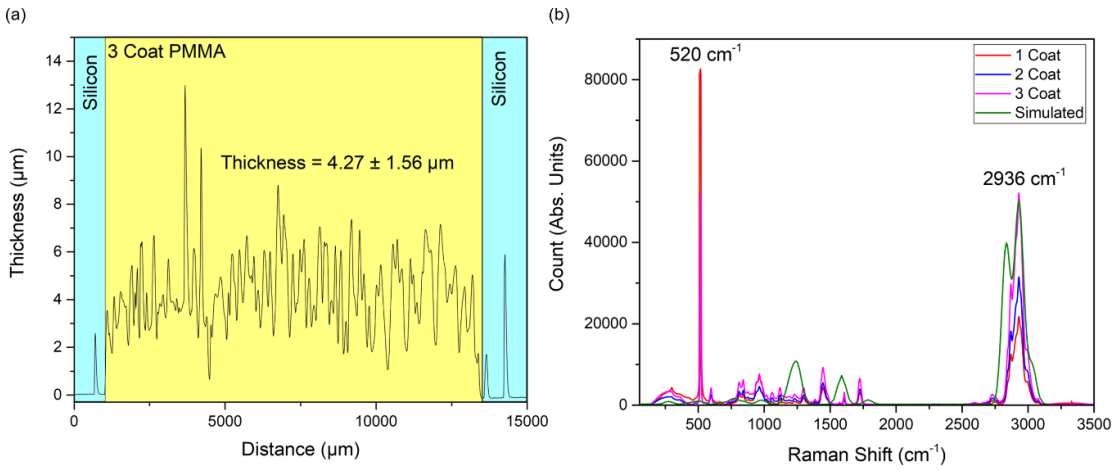

Figure 2. (a) Thickness profile of 3 coat PMMA/c-Si substrates across a 1 cm^2 area. The colourisation of the different areas is for visual aid only (b) Raman spectra of PMMA/c-Si for a 1,2, and 3 coat PMMA film, along with the simulated Raman spectrum for MMA.

averaged profilometry measurement of the 1 cm^2 3 coat PMMA encapsulation on crystalline silicon (c–Si). Here, the PMMA film is still inhomogeneous as demonstrated by the significant thickness variation. From the profilometry measurements, the PMMA thickness was calculated to be 4.27 $\pm$ 1.56 μm across a total distance of $\sim$12 000 μm (12 mm).

To improve the thickness estimation, Raman spectroscopy measurements were performed. As the PMMA encapsulation has high transparency in the visible range, the Raman signal from the PMMA films can be correlated to the thickness of the layer as the laser is not readily absorbed by the film [29]. To remove any overlap of Raman signal from the underlying substrate, 3 coats of PMMA was sprayed onto a silicon substrate using a 1 cm^2 mask. Figure 2(b) shows the Raman spectra for 1,2, and 3 coats of PMMA on silicon substrates. The Raman spectra for Methyl Methacrylate (MMA) was simulated via ORCA to assign the Raman peaks [30], and the Raman mapping data is shown in figure S.5.

In figure 2(b), the Raman peak from the silicon (520 cm^{-1}) is visible for all samples, indicating that the PMMA layer has not readily absorbed the laser. Setting the film thickness to be proportional to the intensity of the 2936 cm^{-1} PMMA peak, which through DFT simulations is C-H symmetric stretching, the film thickness for 1 and 2 coats of PMMA (using the thickness of 3 coats measured in figure 2(a)) were calculated to be 1.77 $\pm$ 0.63 μm and 2.57 $\pm$ 0.92 μm respectively. At a thickness of 1.77 μm, samples weighed before and after showed the encapsulation layer possess a weight of $\sim$6 mg, and at 3 coats the encapsulation weighs $\sim$15 mg. Due to the low weight of the encapsulation, it increases the specific power of the PSCs significantly as the encapsulation only accounts for 0.4% of the total device weight compared to $\sim$50% in a glass-glass encapsulation technique. It is also $\sim$283$\times$ lighter than the glass ($\sim$1.7 g). The roughness of the silicon substrate was measured through Atomic Force Microscopy (AFM), as shown in figure S.4. Here, the Root Mean Square (RMS) roughness (Rq) of the silicon was calculated as 0.376 nm. Therefore, the inhomogeneity of the PMMA thickness is unlikely due to the roughness or defects in the substrate, and more likely due to the coating method as the spray can does not offer consistent pressure during each pass. The Scanning electron microscopy (SEM) images obtained for the same 3 coat sample measured under profilometry to show the inhomogeneity and the PMMA/silicon interface are shown in figure S.5.

2.3. Stability testing

A key requirement for encapsulation is to reduce moisture and oxygen permeating into the device and actively degrading performance. This is especially true when samples are held in storage. To investigate the stability of PSCs using PMMA encapsulation, two experiments were performed under different humidity conditions.

The primary experiment consisted of 1 coat PMMA/PSCs in the dark storage at ambient conditions ($\sim$40%–45% RH $\sim$25 °C) (ISOS-D1), and were periodically measured to investigate any changes in performance and thus stability. Un-encapsulated samples were also placed in the same container to act as controls. The dark conditions removed any photo-activated degradation effects and the conditions inside the storage container were measured with a temperature and humidity data-logger (DT-1700, ATP). These conditions also mimic the storage of devices during waiting periods between fabrication and application. The results are shown in figure 3.

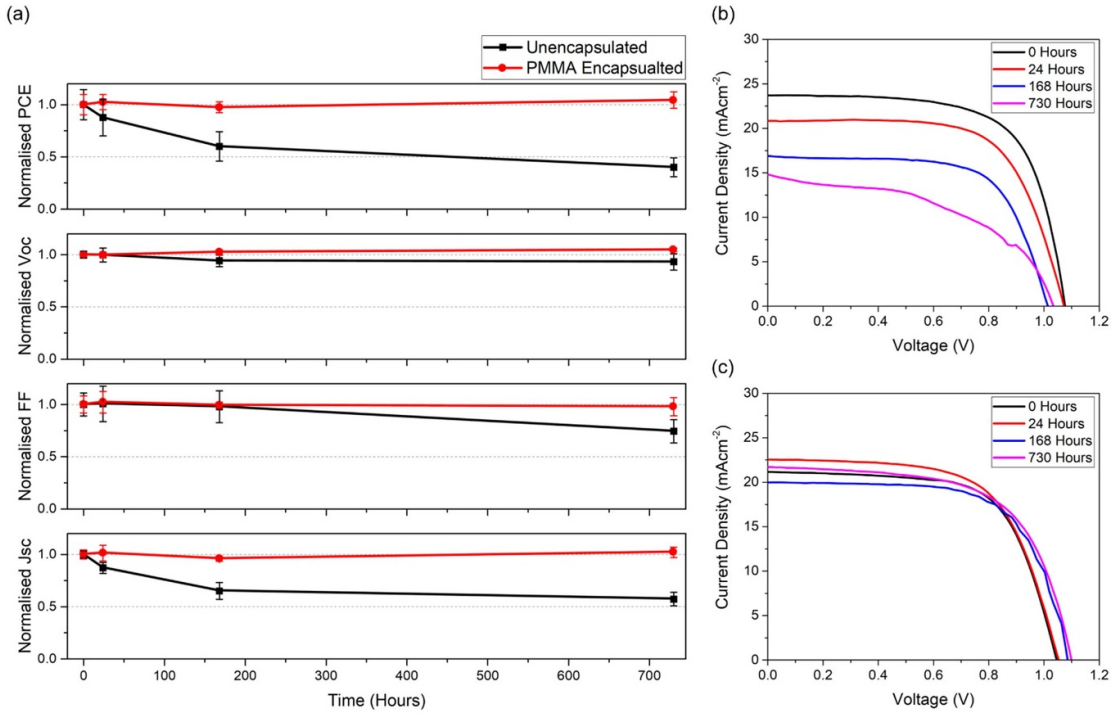

Figure 3. (a) Normalised device parameters for an un-encapsulated and 1 coat PMMA/PSCs in dark storage and under ambient conditions as a function of storage time. Raw data is shown in table S.3 in SI. (b) J–V curves for the champion unencapsulated control device as a function of storage time. (c) J–V curves for the champion 1 coat PMMA encapsulated device as a function of storage time.

Here it is shown that the inclusion of the 1 coat PMMA encapsulation greatly improves the overall stability of the PSCs. Under ambient conditions, the PMMA/PSCs show a 100% PCE retention after 730 h of testing, while the control devices show an averaged PCE retention of 40%. The decrease in device performance for the control devices is largely driven by the 43% decrease in J_{sc}, and 26% decrease in FF. The average V_{oc} of the control devices decreased by 7% after 730 h.

Figure 3(b) and (c) show the corresponding JV curves. For the PMMA encapsulated devices, the J_{sc} increased by 2%, while the FF decreased by 2%. The V_{oc} increased by 5% for the PMMA/PSCs. Overall, after 730 h of dark ambient stability testing, the PMMA/PSCs showed a 60% improvement in PCE retention compared to the control devices, indicating a reduction in moisture and oxygen permeation into the perovskite devices. There is a small improvement in device PCE after the 730 h testing which is attributed to positive moisture presence within the device. As PMMA has a WVTR, moisture will slowly enter the device over time. It has been shown that the presence of moisture within the perovskite active material promotes a positive reaction between the PbI_2 and organic salts [31, 32]. This reaction leads to defect and thus an improvement in the V_{oc}, which is also seen above. It has also been shown that the inclusion of H_20 can improve performance of triple cation PSCs by improving the crystallinity of the perovskite [33]. However, too much moisture will eventually degrade the perovskite material as seen in the un-encapsulated devices.

As the permeation of moisture and oxygen are inversely proportional to the film thickness, a 3 coat PMMA/PSC should offer better stability than 1 coat at harsher conditions (85% RH). To study this, the second experiment investigated the stability of 1 and 3 coat PMMA/PSCs placed in a humidity oven (HCP50, Memmert) at 85% RH 25 °C. These conditions are similar to ISOS-D3; however, the temperature was reduced to limit complications due to the possible thermal degradation of the spiro-OMeTAD HTM. Here, un-encapsulated devices were again tested alongside the PMMA/PSCs to act as controls. In conjection, 1 and 3 coat PMMA/PSCs were tested to probe the humidity stability as a function of PMMA thickness. The normalised PCE is shown in figure 4, with the remaining PV parameters shown in figure S.6. The raw data can is presented in tables S.4 and S.5 in the SI.

The inclusion of the PMMA encapsulation greatly improves the stability of PSCs even at 85% RH. After 50 h of testing, the control samples show a ∼95% loss in PCE and is completely degraded after 168 h of testing. This loss in PCE is driven by a similar loss in J_{sc} (80% and 90% respectively). At the same time intervals, both the 1 & 3 coat PMMA/PSCs show ∼100% PCE retention after 50 h. However, the 1 coat PMMA/PSCs degrades by 30% after 168 h of testing, with this decrease in performance arising from a ∼10%,

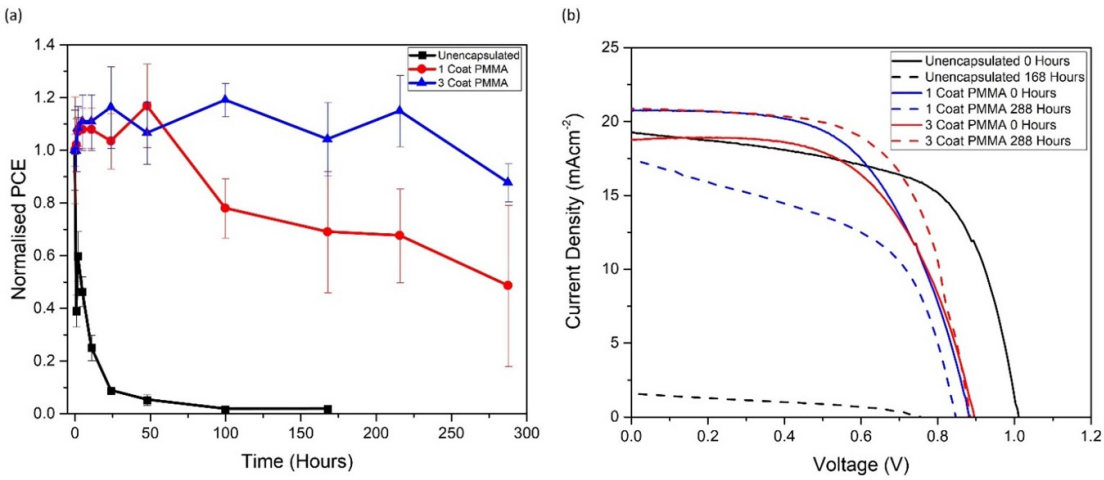

Figure 4. (a) Normalised PCE for an unencapsulated, 1, and 3 coat PMMA/PSCs under 85% RH 25 °C. Raw data is shown in SI tables S.4. and S.5. (b) J-V curves for the champion devices before and after 288 h of 25 °C 85% RH humidity treatment.

∼18%, and ∼10% reduction in V_{oc}, FF, and J_{sc} respectively (figure S.6). The 3 coat PMMA/PSCs exhibit ∼100% PCE retention after 168 h, and 88% PCE retention after 280 h. After 200 h, the 3 coat PMMA samples PCE improves by 15% on average which is attributed to a similar positive moisture mechanism seen in figure 3. Here, the time scale is much faster and is attributed to the increased relative humidity compared to figure 3.

Figure 4(b) shows the JV curves for the champion devices before and after 288 h of 85% RH 25 °C humidity treatment. The difference in degradation rate between the 1 & 3 coat PMMA/PSCs demonstrates how the stability of the PMMA/PSCs is impacted by the thickness of the encapsulation layer. Additionally, it is plausible that a more homogeneous encapsulation layer will further increase the stability as there will be less variation in the WVTR across the film.

Additionally, a preliminary experiment further investigating the affect of PMMA thickness on moisture stability was also performed. Here, perovskite devices were submerged into a beaker of H_2O. The results of this experiment are presented in supplementary information figures 7 and 8. From the first results, the thicker the PMMA layer the better the water stability. This should be properly investigated in future work through contact angle measurements.

3. Conclusion

Moisture and oxygen experienced in normal working and storage conditions induces degradation in PSCs that hamper the stability. We selected PMMA in ethyl acetate as a potential encapsulation choice due to it possessing a high vapour pressure, reducing the degradation of the layers underneath the encapsulant. We reported a 1 coat PMMA encapsulation thickness of 1.77 ± 0.63 μm with a measured weight of 6 mg, therefore greatly increasing the specific power. Spray-coating the PSCs with a PMMA encapsulation results in an improvement under ISOS-D1 conditions, without the loss of device performance as a result of the encapsulation process. PMMA encapsulated PSCs show an improved stability after 730 h of ambient storage, with 100% PCE retention compared to a 60% PCE loss for the un-encapsulated devices. Under 85% RH 25 °C stability testing, the importance of encapsulation thickness becomes apparent as the thicker PMMA encapsulated devices showed better stability (88% PCE retention) and performance retention than thinner layers (49% PCE retention) after ∼300 h. Our work identifies a new strategy for encapsulating PSCs, while also improving ambient stability, high humidity stability, and increasing the specific power. Future work utilising this encapsulation technique will look to improve the uniformity of the film coating through methods such as ultrasonic spraying [34], and by changing the solvent mixture the PMMA is dissolved in to assess coating efficiencies and to compare to commercial products.

4. Methods

4.1. Preparation and fabrication of planar PSCs

ITO coated soda lime glass (Lumtec, Taiwan) were cleaned via ultrasonication in Hellmanex (2%, deionized water), deionized water, acetone, and then 2-propanol before being dried via a N_2 stream. The substrates were treated in oxygen plasma. A planar layer of SnO_2 at a thickness of ∼25 nm was subsequently deposited via spin-coating at a spin speed of 3000 rpm and an acceleration of 3000 rpm for 30 s. This was followed by sintering the substrates at 150 °C for 30 min in a fume hood. Triple-cation perovskite films were deposited in an N_2 atmosphere using single-step deposition method from the precursor solution containing FAI, PbI_2, MABr, and PbBr2 in anhydrous N,N-dimethyl formamide/dimethyl sulphoxide. Thereafter, 53 μl of CsI was added to the precursor solution. The precursor solution was spin-coated onto the planar SnO_2 films in a two-step program. During the second step, 300 μl of chlorobenzene was dropped on the spinning substrate. This was followed by annealing the films at 100 °C for 1 h. To complete the fabrication of devices, 2,20,7,70-tetrakis(N,N-di-p-methoxyphenylamine)-9,9-spirobifluorene (Spiro-OMeTAD) as a hole transporting material was deposited by spin-coating. The Spiro-OMeTAD solutions was doped with bis(trifluoromethane)sulfonimide lithium salt (99.95%; Sigma-Aldrich) dissolved in acetonitrile, tris(2-(1 H-pyrazol-1-yl)-4-tertbutylpyridine)-cobalt(III)-tris(bis(trifluoromethylsulfonyl)imide) (FK 209) and 4-tert-butylpyridine. Finally, device fabrication was completed by thermally evaporating a gold layer as a back contact. The full deposition methods for the SnO2, triple cation perovskite, the spiro-OMeTAD HTL, and the gold contact follow the same procedures as outline in other literature [35]. The Glass–Glass encapsulation was performed by applying a 20 × 24 mm strip of Kapton tape over the pixels, followed by the application of UV cured epoxy. 20 × 24 mm plain Glass was placed onto the epoxy and it was cured for 7 min under UV light. The devices with Glass–Glass encapsulation are only shown in the supplementary information figure S.1.

4.2. Spray encapsulation

Ambersil Acrylic Conformal Coating (RS Components, UK) was used to encapsulate the PSCs. The spray cans were used as bought and were not altered in any way. The PMMA solution has a quoted bulk viscosity of 10–20 mPa·s. The PMMA was sprayed onto PSCs at a spray height of 40 cm from the samples. The PSCs were placed on a hotplate set to 55 °C, with a 20 × 24 mm masked placed on top to reduce any shadowing of the PMMA spray. 2 passes over the sample was denoted 1 coat, 4 passes 2 coats, and 6 passes 3 coats. The samples were kept on the hotplate for 5 min after spraying to allow for the PMMA to dry.

4.3. Characterisation

J–V Characterization: The J–V characteristics of perovskite devices were recorded with a digital source meter (Keithley model 2400, USA) and 450 W xenon lamp (Sol3A Class AAA Solar Simulator; Oriel, USA). The light source was equipped with an AM1.5 G air mass filter. Both forward- and reverse bias scans were taken from 1.2 to −0.1 V with a sweep interval of 0.015 V [35].

Thickness Characterisation: The profilometry thickness measurements were taken using the Alpha Step D-500 stylus profilometer (KLA Tencor). The diamond tipped stylus force was set to 5 mg, and the maximum height range was set at 10 μm. For each sample, 3 measurements were taken at different locations and the Alpha-Step software included with the profilometer automatically calculated the average and standard deviation of the measured thicknesses.

Raman: Raman measurements were performed with a Renishaw inVia Raman system (Renishaw plc., Wotton-Under-Edge, UK) in backscattering configuration. A 532 nm laser and 50× objective were used (NA 0.50, spot size ∼1 μm). For Raman measurements, a laser power of 150 μW and acquisition time of 10 s were used to measure 25 different points, which were averaged in a single spectrum.

AFM: AFM measurements were performed with a JPK NanoWizard 3. c-Si wafers were scanned by the AFM over areas of 10 μm × 10 μm in tapping mode. The scanning images were analysed by Gwyddion software (Version 2.55) to determine the surface roughness parameters.

SEM: SEM images were produced using a Hitachi TM4000 plus microscope and Hitachi map 3D software. Images were obtained using a backscatter detector, an accelerating voltage of 15 kV and a working distance of 10 mm. Samples were attached to the stage by carbon tape and charge reduction mode was used to reduce charging of the sample surface.

Data availability statement

All data that support the findings of this study are included within the article (and any supplementary files).

Acknowledgments

The authors would like to thank Airbus Endeavr Wales for their financial support. The authors would also like to thank the EPSRC through the ATIP (EP/T028513/1) Grant and the SPECIFIC Innovation and Knowledge Centre Phase 2 (EP/N020863/1). The IMPACT operation has been part-funded by the European Regional Development Fund through the Welsh Government and Swansea University. M S is funded through an EPSRC ICASE scholarship in collaboration with IQE plc. The manuscript was written through contributions from all authors. All authors have given approval to the final version of the manuscript.

Author contributions

D H and M S designed the research. D H and M S fabricated the standard (NIP) planar PSCs. D H and M S spray coated the PMMA. D H, R A, S K T, and M S performed the electrical characterisation and analysis. D H performed the profilometry measurements, and ambient dark storage measurements. M S performed the dark humid lifetime measurements. D H performed Raman spectroscopy. S K T performed and analysed the AFM measurements. C G performed and analysed the SEM measurements. M J C, and W C T supervised the research, along with providing many insightful remarks and suggestions. All authors discussed the results and commented on the manuscript.

Conflict of interest

The authors declare no competing interests.

ORCID iDs

Declan Hughes https://orcid.org/0000-0001-6415-3717
Rokas Apanavicius https://orcid.org/0009-0006-2582-9562
Matthew J Carnie https://orcid.org/0000-0002-4232-1967
Wing C Tsoi https://orcid.org/0000-0003-3836-5139

References

[1] Gong J, Darling S and You F 2015 Perovskite photovoltaics: life-cycle assessment of energy and environmental impacts *Energy Environ. Sci.* **8** 1953–68
[2] Song Z, McElvany C, Phillips A, Celik I, Krantz P, Watthae S, Liyanage G K, Apul D and Heben M J 2017 A technoeconomic analysis of perovskite solar module manufacturing with low-cost materials and techniques *Energy Environ. Sci.* **10** 1297–305
[3] Snaith H J 2018 Present status and future prospects of perovskite photovoltaics *Nat. Mater.* **17** 372–6
[4] Liu S-C, Li Z, Yang Y, Wang X, Chen Y-X, Xue D-J and Hu J-S 2019 Investigation of oxygen passivation for high-performance all-inorganic perovskite solar cells *J. Am. Chem. Soc.* **141** 18075–82
[5] Qiao L, Fang W-H, Prezhdo O V and Long R 2022 Suppressing oxygen-induced deterioration of metal halide perovskites by alkaline earth metal doping: a quantum dynamics study *J. Am. Chem. Soc.* **144** 5543–51
[6] Xu H A 2020 Brief review on the moisture stability for perovskite solar cells *IOP Conf. Ser.: Earth Environ. Sci.* **585** 012027
[7] Gangishetty M K, Scott R W and Kelly T L 2016 Effect of relative humidity on crystal growth, device performance and hysteresis in planar heterojunction perovskite solar cells *Nanoscale* **8** 6300–7
[8] Lochhead K, Johlin E and Yang D 2022 Encapsulation of perovskite solar cells with thin barrier films *Thin Films* ed D Yang (*Deposition Methods and Applications*) (IntechOpen) pp 105–20
[9] Li J *et al* 2021 Encapsulation of perovskite solar cells for enhanced stability: structures, materials and characterization *J. Power Sources* **485** 229313
[10] Aitola K, Gabriela Sonai G G, Markkanen M, Kaschuk J J, Hou X, Miettunen K and Lund P D 2022 Encapsulation of commercial and emerging solar cells with focus on perovskite solar cells *Sol. Energy* **237** 264–83
[11] Boyd C C, Cheacharoen R, Leijtens T and McGehee M D 2018 Understanding degradation mechanisms and improving stability of perovskite photovoltaics *Chem. Rev.* **119** 3418–51
[12] Ramasamy E, Karthikeyan V, Rameshkumar K and Veerappan G 2019 Glass-to-glass encapsulation with ultraviolet light curable epoxy edge sealing for stable perovskite solar cells *Mater. Lett.* **250** 51–54
[13] Barbé J, Pockett A, Stoichkov V, Hughes D, Lee H K H, Carnie M, Watson T M and Tsoi W C 2020 In situ investigation of perovskite solar cells' efficiency and stability in a mimic stratospheric environment for high-altitude pseudo-satellites *J. Mater. Chem.* C **8** 1715–21
[14] Biyu L, Xianzi Z, Huafeng C, Renjie C, Nannan H, Lina C, Penghui F and Xiaohong C 2022 Excellent stability of perovskite solar cells encapsulated with paraffin/ethylene-vinyl acetate/paraffin composite layer *Front. Mater.* **9** 892657
[15] McKenna B, Troughton J R, Watson T M and Evans R C 2017 Enhancing the stability of organolead halide perovskite films through polymer encapsulation *RSC Adv.* **7** 32942–51
[16] Porter C E and Blum F D 2000 Thermal characterization of PMMA thin films using modulated differential scanning calorimetry *Macromolecules* **33** 7016–20
[17] Zafar M S 2020 Prosthodontic applications of polymethyl methacrylate (PMMA): an update *Polymers* **12** 2299
[18] Fidan S 2014 Tribological performance of polymethyl methacrylate as an aviation polymer *J. Polym. Eng.* **34** 569–79

[19] Su W, Cook B S, Fang Y and Tentzeris M M 2016 Fully inkjet-printed microfluidics: a solution to low-cost rapid three-dimensional microfluidics fabrication with numerous electrical and sensing applications *Sci. Rep.* **6** 35111
[20] Wilderspin T J, De Rossi F and Watson T M 2016 A simple method to evaluate the effectiveness of encapsulation materials for perovskite solar cells *Sol. Energy* **139** 426–32
[21] Han G S, Yoo J S, Yu F, Duff M L, Kang B K and Lee J K 2017 Highly stable perovskite solar cells in humid and hot environment *J. Mater. Chem.* A **5** 14733–40
[22] Zhang M, Zhang F, Shi K, Zhang W, Huang J and Qiu H 2022 Polymer passivation of defects in inorganic perovskite solar cells *Optoelectron. Lett.* **18** 338–42
[23] Kim H, Lee K S, Paik M J, Lee D Y, Lee S-U, Choi E, Yun J S and Seok S I 2022 Polymethyl methacrylate as an interlayer between the halide perovskite and copper phthalocyanine layers for stable and efficient perovskite solar cells *Adv. Funct. Mater.* **32** 2110473
[24] Rathinavelu U, S. J M, Moller P and Ambat R 2012 Effect of no-clean flux residues on the performance of acrylic conformal coating in aggressive environments *IEEE Trans. Compon. Packag. Manuf. Technol.* **2** 719–28
[25] Corsini F and Griffini G 2020 Recent progress in encapsulation strategies to enhance the stability of organometal halide perovskite solar cells *J. Phys. Energy* **2** 031002
[26] Isabelli F, Di Giacomo F, Gorter H, Brunetti F, Groen P, Andriessen R and Galagan Y 2018 Solvent systems for industrial-scale processing of spiro-OMeTAD hole transport layer in perovskite solar sells *ACS Appl. Energy Mater.* **1** 6056–63
[27] Bu T *et al* 2017 Synergic interface optimization with green solvent engineering in mixed perovskite solar cells *Adv. Energy Mater.* **7** 1700576
[28] Hülsmann P, Weiß K-A and Köhl M 2014 Measurement and modelling of water ingress into double-glass photovoltaic modules *Prog. Photovolt. Res. Appl.* **22** 415–21
[29] Li S-L, Miyazaki H, Song H, Kuramochi H, Nakaharai S and Tsukagoshi K 2012 Quantitative Raman spectrum and reliable thickness identification for atomic layers on insulating substrates *ACS Nano* **6** 7381–8
[30] Neese F 2017 Software update: the orca program system, version 4.0. *Wiley Interdiscip. Rev. Comput. Mol. Sci.* **8** e1327
[31] Fan W, Deng K, Shen Y, Bai Y and Li L 2022 Moisture-accelerated precursor crystallisation in ambient air for high-performance perovskite solar cells toward mass production *Angew. Chem., Int. Ed.* **134** e202211259
[32] Liu K *et al* 2022 Moisture-triggered fast crystallization enables efficient and stable perovskite solar cells *Nat. Commun.* **13** 4891
[33] Zhang W, Xiong J, Li J and Daoud W A 2019 Mechanism of water effect on enhancing the photovoltaic performance of triple-cation hybrid perovskite solar cells *ACS Appl. Mater. Interfaces* **11** 12699–708
[34] Lonakar G S, Mahajan M S , Ghosh S S and Sali J V 2012 Modeling thin film formation by ultrasonic spray method: a case of PEDOT:PSS thin films *Org. Electron.* **13** 2575–81
[35] Barbé J, Hughes D, Wei Z, Pockett A, Lee H K H, Heasman K C, Carnie M J, Watson T M and Tsoi W C 2019 Radiation hardness of perovskite solar cells based on aluminum-doped zinc oxide electrode under proton irradiation *Phys. Status Solidi* **3** 1900219